JCIM JOURNAL OF CHEMICAL INFORMATION AND MODELING

pubs.acs.org/jcim
Article

Conformational Signatures of Preassembled and Active Complexes of 5-HT$_7$ with the G$_s$ Protein

Zeenat Zara,[▽] Alessandro Nicoli,*[,▽] Ruiming He, Natalia Kulik, David Reha, Alexey Bondar, and Antonella Di Pizio*

Cite This: J. Chem. Inf. Model. 2025, 65, 11826−11836
Read Online

ACCESS | Metrics & More | Article Recommendations | Supporting Information

ABSTRACT: 5-Hydroxytryptamine receptor type 7 (5-HT$_7$) receptor is a G protein-coupled receptor (GPCR) exhibiting noncanonical signaling properties. It has been shown that 5-HT$_7$ can form stable inactive preassembled complexes with its cognate G$_s$ protein. Structural determinants of such complex formation and the distinction between preassembled and intermediate activated complexes remain unknown. Here, we use molecular modeling and molecular dynamics simulations to determine and characterize the binding interface between this receptor and the G$_s$ protein in both the active and preassembly complexes. Our results show key interaction patterns specific for the different states and pinpoint unique structural features distinguishing active, inactive, and preassembled states of the receptor.

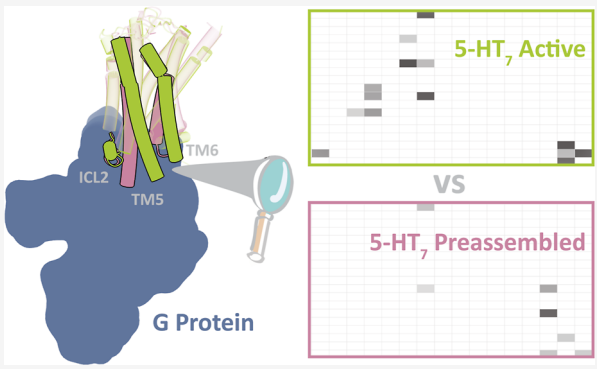

1. INTRODUCTION

The 5-hydroxytryptamine receptor type 7 (5-HT$_7$) receptor is a signaling protein widely expressed in glial cells and neurons throughout the central nervous system, including the spinal cord, thalamus, hypothalamus, amygdala, and suprachiasmatic nucleus,[1−4] where it is involved in many physiological activities, including the sleep cycle, circadian rhythm, rapid eye movement, thermoregulation, and memory.[1,5] In the gastrointestinal tract, 5-HT$_7$ is expressed in immune cells in lymphoid tissues, where it plays a role in the inflammation response.[6] Dysregulation of 5-HT$_7$ signaling may cause various pathological conditions, including neurodegenerative diseases, cognitive disorders, depression, and immune system-related diseases.[6,7] Therefore, 5-HT$_7$ represents an intriguing target for therapeutic applications.

5-HT$_7$ is a member of the G protein-coupled receptor family (GPCR), a family of membrane proteins that are targeted by 34% of approved drugs.[8,9] 5-HT$_7$ belongs to the serotonin subfamily of class A GPCRs. Humans express 7 types of 5-HT receptors: 5-HT$_1$ (5-HT$_{1A}$, 5-HT$_{1B}$, 5-HT$_{1C}$, 5-HT$_{1D}$, 5-HT$_{1E}$, 5-HT$_{1F}$), 5-HT$_2$ (5-HT$_{2A}$, 5-HT$_{2B}$, 5-HT$_{2C}$), 5-HT$_3$, 5-HT$_4$, 5-HT$_5$, 5-HT$_6$, and 5-HT$_7$,[10] which are all GPCRs with the exception of 5-HT$_3$ that is an ionotropic receptor. GPCRs signal primarily through the activation of heterotrimeric G proteins composed of α, β, and γ subunits. Upon agonist binding, e.g., serotonin (5-hydroxytryptamine, 5-HT), to 5-HT receptors, the receptor undergoes conformational changes leading to the recruitment of a G protein.[11,12] The activation of the G protein results in the dissociation of the G$_\alpha$ subunit from the G$_{\beta\gamma}$ and subsequent attenuation of downstream pathways.[13] The 16 human genes encoding G$_\alpha$ proteins are categorized into four major families: G$_S$ (G$_s$ and G$_{olf}$), G$_{i/0}$ (G$_{i1}$, G$_{i2}$, G$_{i3}$, G$_o$, G$_z$, G$_{t1}$, G$_{t2}$, and G$_{gust}$), G$_{q/11}$ (G$_q$, G$_{11}$, G$_{14}$, and G$_{15}$), and G$_{12/13}$ (G$_{12}$ and G$_{13}$). The 5-HT receptor subtypes vary in their primary coupling. 5-HT$_1$ and 5-HT$_5$ couple to G$_{i/0}$, 5-HT$_2$ to G$_{q/11}$, and 5-HT$_4$, 5-HT$_6$, and 5-HT$_7$ couple to the G$_S$.[14]

In addition to the canonical G protein coupling, 5-HT$_7$ and several other GPCRs can engage with G proteins in the inactive state.[15−24] This mode of coupling is termed precoupling, preassembly, or inverse coupling. 5-HT$_7$ forms a long-lasting inactive complex with the G$_s$ protein,[18] which has been proposed to downregulate the intrinsic basal activity of 5-HT$_7$.[19,22]

The structure of 5-HT$_7$ in the active state in complex with its downstream partner G$_s$ protein has been released,[29] however structural insights into the inactive state and preassembled complex are still lacking. Understanding the molecular basis of 5-HT$_7$ signaling will be valuable for the design of precise modulators of this receptor. In this work, we characterized snapshots of the major conformational states of 5-HT$_7$ by integrating molecular modeling and molecular dynamics (MD) simulations. MD simulations have been successful in revealing

Received: July 18, 2025
Revised: September 22, 2025
Accepted: September 23, 2025
Published: October 24, 2025

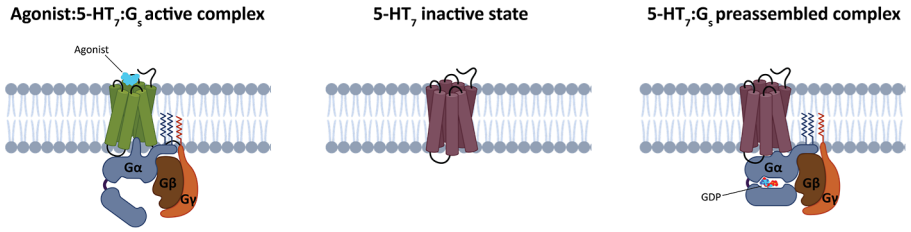

Figure 1. Schematic representation of the three states modeled and simulated in this study. 5-HT_7 is colored in green in the active state and dark purple for the inactive state. The G protein subunits α, β, and γ are colored in blue, brown, and orange, respectively. The active state was simulated in the presence of the cocrystallized agonist, while the preassembled state in the presence of the guanosine diphosphate (GDP).

transient interactions and the inherent flexibility, such as breathing motions, of GPCRs, even over relatively short time scales.[25,26] Our MD analysis enabled the identification of unique, state-specific contact patterns and conformational features that regulate the 5-HT_7:G_s preassembled complex. This provides insights into the functional role of this state in the activation mechanism of 5-HT_7.

2. RESULTS AND DISCUSSION

Upon activation, 5-HT_7 undergoes a conformational change from the inactive to the active state and interacts with the G_s protein heterotrimer ($G_{\alpha\beta\gamma}$). The formation of the fully activated complex catalyzes the exchange of guanosine diphosphate (GDP) for guanosine triphosphate (GTP) on the G_α subunit and subsequently activates downstream signaling pathways.[27] In the inactive state, 5-HT_7 can associate with the GDP-bound heterotrimeric G_s protein and form a stable complex.[18] In our study, we combined molecular modeling and MD simulations for a comprehensive structural analysis of the active state of 5-HT_7 in complex with the nucleotide-empty G_s protein, the inactive state of 5-HT_7 and the preassembled 5-HT_7:G_s complex (Figure 1).

To facilitate structural analyses and comparisons, throughout this work, we use numbering systems and terminology specifically developed for GPCRs and G proteins. All GPCRs share a common structural architecture of seven transmembrane (7TM) α-helices connected by three intracellular loops (ICL1, ICL2, and ICL3) and three extracellular loops (ECL1, ECL2, ECL3).[11] According to the Ballesteros−Weinstein (BW) numbering scheme, TM residues are numbered referring to the highest conserved residue of each TM as the position X.50 (X indicates helix number).[28] The G_α subunit consists of two main domains: a Ras domain (RD) that is involved in the binding and hydrolysis of GTP and the helical domain (HD) that buries the GTP within the core of the protein (Figure S1). The RD is composed of six β (β1−β6) strands and five α-helices (H1−H5). The HD consists of six α-helices (HA−HF) that are inserted between H1 and β2 of the Ras domain. A αN helix (HN) is located before the Ras domain. Residues belonging to RD, HN, and HD are numbered according to their position in the secondary structure, e.g., the first residue of the α5 helix is residue position G.H5.01, where G represents the G_α subunit, G.H5 represents the α5 helix, and the 01 stands for the first residue of the α5 helix. Similarly, the position G.S6.03 represents the third residue of the β6 strand, where S6 reflects the β6 strand and 03 represents the third residue of this β6 strand. Loop regions are commonly named based on structured regions present before and after that loop, for example, the residue $S84^{G\text{-}h1ha.20}$ is a loop region between H1 and HA, and 20 stands for the 20th residue of this loop, whereas $A48^{G\text{-}s1h1.02}$ is a loop residue between β1 and H1 and the 02 is the second residue of this loop. In the case of loop regions, small letters are used to refer to the structured regions.

2.1. Preassembled and Active Complex of the 5-HT_7 Receptor with the Heterotrimeric G_s Protein. The preassembled complex is formed between inactive 5-HT_7 and inactive GDP-bound G_s protein (Figure 1). As the structure of 5-HT_7 is experimentally available only in the active state,[29] we modeled the 5-HT_7 structure in the inactive state (Figure S2). We then modeled the preassembled complex between the inactive 5-HT_7 with the refined inactive G_s protein bound to GDP, following a previous computational study on preassembled complexes of 5-HT_{1A} and other class A GPCRs.[30,31] In the modeled preassembled complex, G.H5 is not deeply inserted into the intracellular side of 5-HT_7 due to the inward position of TM6, which occludes the G protein binding site (Figure 2). The G.H5 has a pivotal role on GPCR activation, it fully extends inside the intracellular side of the GPCR and initiates allosteric conformational alterations in proximity to the nucleotide-binding pocket, resulting in GDP release and the opening of the HD.[32] Instead, H5 in the preassembled complex has a different angle of tilt of the α-helix compared to its conformation in the G_s nucleotide free state (Figure 2). Because of these differences, the interface of the full active complex is much wider (4035 Å^2) compared to the interface of the preassembled complex (3660 Å^2) (Figure S3).

To explore the local flexibility of the fully active and preassembled complexes, we performed MD simulations. We ran five independent replicas of 500 ns for each system (total aggregate time of 5 μs). The Root Mean Square Deviation (RMSD, C_α of each chain vs the initial coordinates) analyses revealed that the complexes are quite stable, even in the modeled regions (Figure S4). To understand the stability of the complexes along the simulations, we monitored the movement of the G_s protein in relation to 5-HT_7 (Figure 2). We observed that G_β and G_γ are more flexible in the preassembled complex than in the fully active complex, due to the local adjustment of the whole G_s protein toward the inactive 5-HT_7 (Figure S4). This suggests that these domains are less involved in the interaction in the preassembled state. While the G_α protein is quite stable throughout the simulation period, we observed a higher flexibility in the region of the long unstructured loop ($V63^{G.h1ha.01}$−$S86^{G\text{-}h1ha.20}$) in the HD for both complexes (as measured by the Root Mean-Square Fluctuation, RMSF, Figure S6). Zooming in on G.H5 ($T369^{G.H5.01}$−$L394^{G.H5.26}$), we observe relatively stable dynamic behavior throughout the simulation in the active complex (Figure 2). This is a consequence of the extensive surface contacts (Figure S3) and multiple interactions that firmly anchor G.H5 to 5-HT_7. The G.H5 conformational space

https://doi.org/10.1021/acs.jcim.5c01698
J. Chem. Inf. Model. 2025, 65, 11826−11836

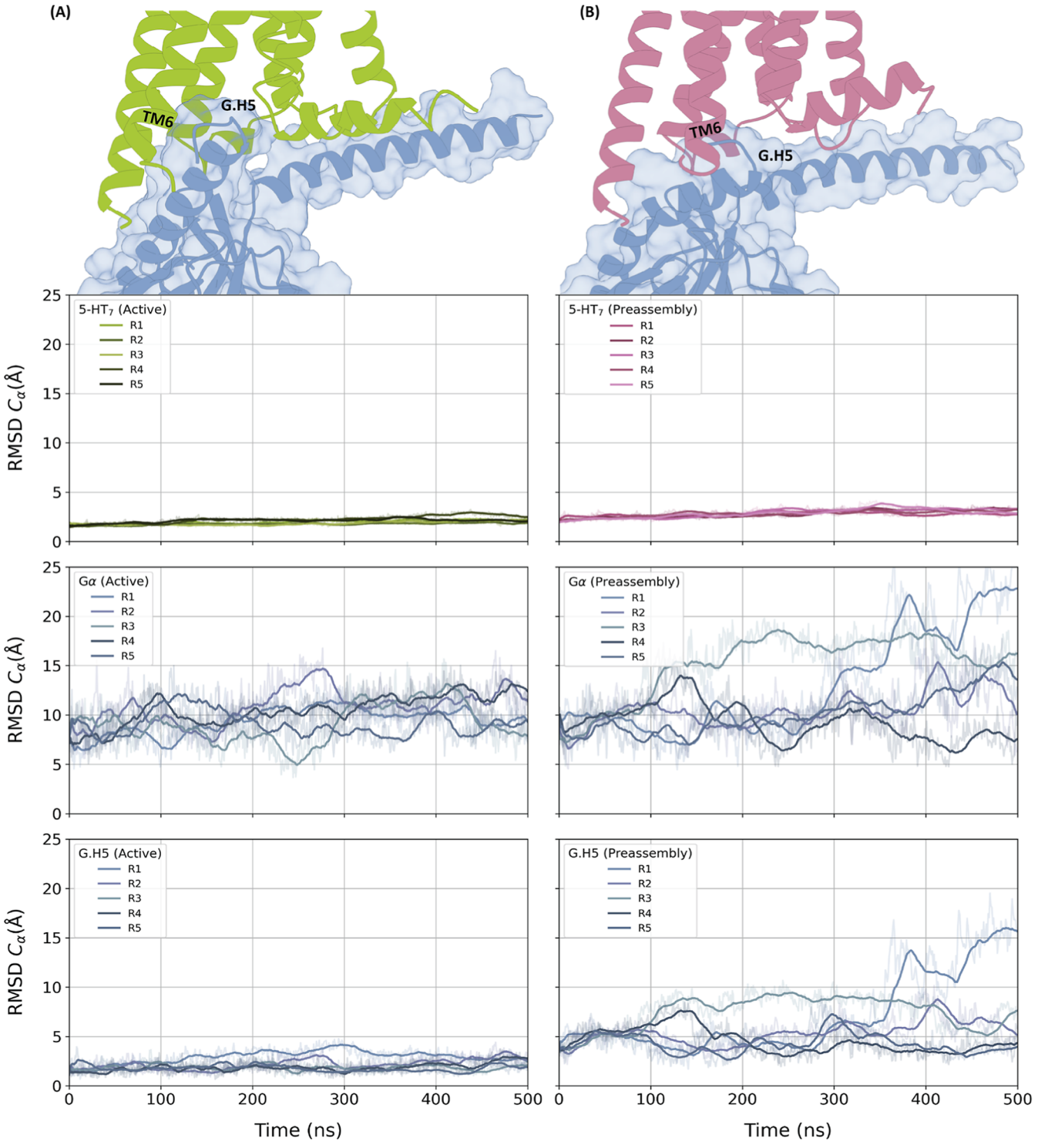

Figure 2. Flexibility of 5-HT$_7$ and G$_s$ during MD simulations. On the top, the representation of the interacting interfaces between 5-HT$_7$ and G$_s$ protein in the fully active (A) and preassembled complexes (B). 5-HT$_7$ is colored in green in the active state and purple for the inactive state. The G protein α subunit is colored in blue. H5 of the G protein and TM6 of 5-HT$_7$ are annotated. The electrostatic surfaces of the complexes are reported in Figure S3. Bottom panels report the root-mean-square deviation (RMSD) plots for 5-HT$_7$, G$_\alpha$, and G.H5 for the active (A) and preassembled complexes (B). The carbon alpha atoms of 5-HT$_7$ (excluding the ICL3 region) were used as the reference for the structural alignment. RMSD plots of all the domains are reported in Figure S4.

sampled in the active complex is more restricted than in the preassembled state (average RMSD is around 5 Å), where side chains continuously adjust throughout the simulation (Figure S7). Moreover, the fully active complex displayed higher peaks in the HB−HE region of the HD domain (E123$^{H.HB.01}$−V184$^{H.HE.1}$, Figure S6). This difference can be attributed to the fact that in the preassembled complex, the helical domain is tightly bound to the GDP and the RD domain, thereby reducing the overall local mobility.

https://doi.org/10.1021/acs.jcim.5c01698
J. Chem. Inf. Model. 2025, 65, 11826−11836

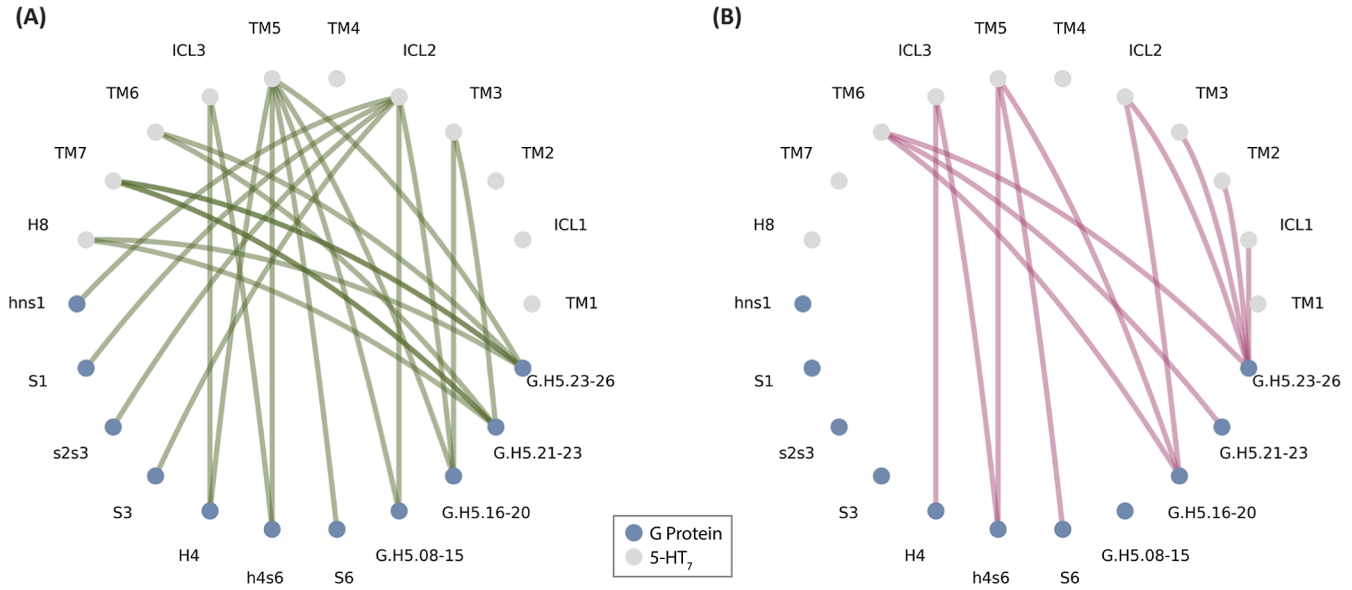

Figure 3. Flare plots representing the interactions between G_α and 5-HT_7 domains in the active (A) and preassembled complex (B). The nodes are colored in blue and gray for the G protein and 5-HT_7 domains, respectively. The edges are colored in green for the interactions in the active complex and in purple for the interactions in the preassembled complex.

2.2. Interaction Interfaces for the Fully Active and Preassembled Complexes. To understand the key contacts that stabilize the complexes, we monitored the interactions between 5-HT_7 and the G_α protein subunit for both active and preassembled complexes. In Figure 3, we report the regions involved in the interaction.

The interacting residues in 5-HT_7 include TM3, ICL2, TM5, TM6, ICL3, TM7, and H8 in the full active complex, whereas TM2, ICL2, TM5, ICL3, and TM6 in the preassembled complex. Therefore, several state-specific interactions are revealed. ICL1 and TM2 residues are involved in interactions in the preassembled complex but not in the fully active state. TM3 residues interact with different residues of H5 in the fully active complex with respect to the preassembled complex. ICL2 interacts exclusively with H5 in the preassembled complex, while, in the active complex, it establishes contacts with different regions of H5 in addition to HN, hns1, S1, S3, and s2s3. TM5 in the active complex establishes contacts with H4 that are absent in the preassembled complex. ICL3 is instead in contact with h4s6 and H4 in both complexes. TM6 residues interact with H5 residues; however, the interacting residues for active and preassembled complexes are different. TM7 and H8 are involved in interactions only in the active complex.

2.3. 5-HT_7 Specificity for the Preassembled Complex and Insights into the Activation Mechanism. Our work revealed several state-specific interactions, many of which emerge and/or become more significant during MD simulations. Figure 4 presents the patterns of interactions in the active (green contour) and preassembled (purple contour) complexes before (Figure S8) and after the simulations.

The G.H5 serves as the primary interacting helix in both the active and preassembled complexes, but our analyses show that the increased protrusion of G_α within the intracellular side of 5-HT_7 in the active state leads to a higher number of interactions of H5 with the receptor compared to the preassembled complex, impacting their local stability (Figure 2). The difference in interactions depends on the different conformations of H5 in the preassembled complex (Figure S7). The RMSD of C_α of G.H5 (residues $T369^{G.H5.01}$–$L394^{G.H5.26}$) between the initial active and preassembled complexes is 6.32 Å. Interestingly, the MD simulations reveal new interactions compared to the experimental structure of the active complex, demonstrating how MD analyses could complement experimental structural data (Figures 4, S8, and S9).[33] Particularly, the H8 of 5-HT_7 increased the number of residues in contact with H5, and ICL2 engaged and established new interactions with H5, HN, S1, the s2–s3 loop, and S3. On the other side, many interactions are maintained in all the MD replicas for the entire simulated time; e.g., the interactions between $Y391^{G.H5.23}$–$R180^{3.50}$, $H387^{G.H5.19}$–$G183^{3.53}$, $Q384^{G.H5.16}$–$I184^{3.54}$, $E392^{G.H524}$–$K324^{6.32}$, and $I383^{H5.15}$ with $P187^{34.50}$ and $L188^{34.51}$ are present in the simulations of the active complex with a frequency of 100%.

Although the structure of the preassembled complex is a model, we found that many of the interactions in the initial structure were retained during the simulations (i.e., $H387^{G.H5.19}$–$G183^{3.53}$, $L346^{G.H4.16}$–$F278^{ICL3}$, and also $P187^{34.50}$ and $P191^{34.54}$ with $L388^{G.H5.20}$). However, new interactions that stabilize the complex appear during the simulations (Figures 4, S8). Specifically, we found that $E322^{6.30}$ interacts with $R385^{G.H5.17}$ and $R389^{G.H5.21}$ residues and the conserved $R180^{3.50}$ with the C-terminus of $L394^{G.H5.26}$ (frequent interactions, >60%). The hydrophobic interactions established between the ICL2 of 5-HT_7 and H5 also increase during the simulations.

Overall, the MD analyses proved to be a valuable tool for optimizing both the preassembled and active complexes. By closely examining key interactions, we identified positions that are highly conserved among all 5-HT receptors, as well as positions that are specific to the 5-HT_7 receptor.

The identified conserved residues are known to play an important role in GPCR activation, which supports the hypothesis of a common activation mechanism for class A GPCRs.[34] $R180^{3.50}$ belongs to the conserved DRY motif and establishes a conserved ionic lock with $E322^{6.30}$, which is also

https://doi.org/10.1021/acs.jcim.5c01698
J. Chem. Inf. Model. 2025, 65, 11826–11836

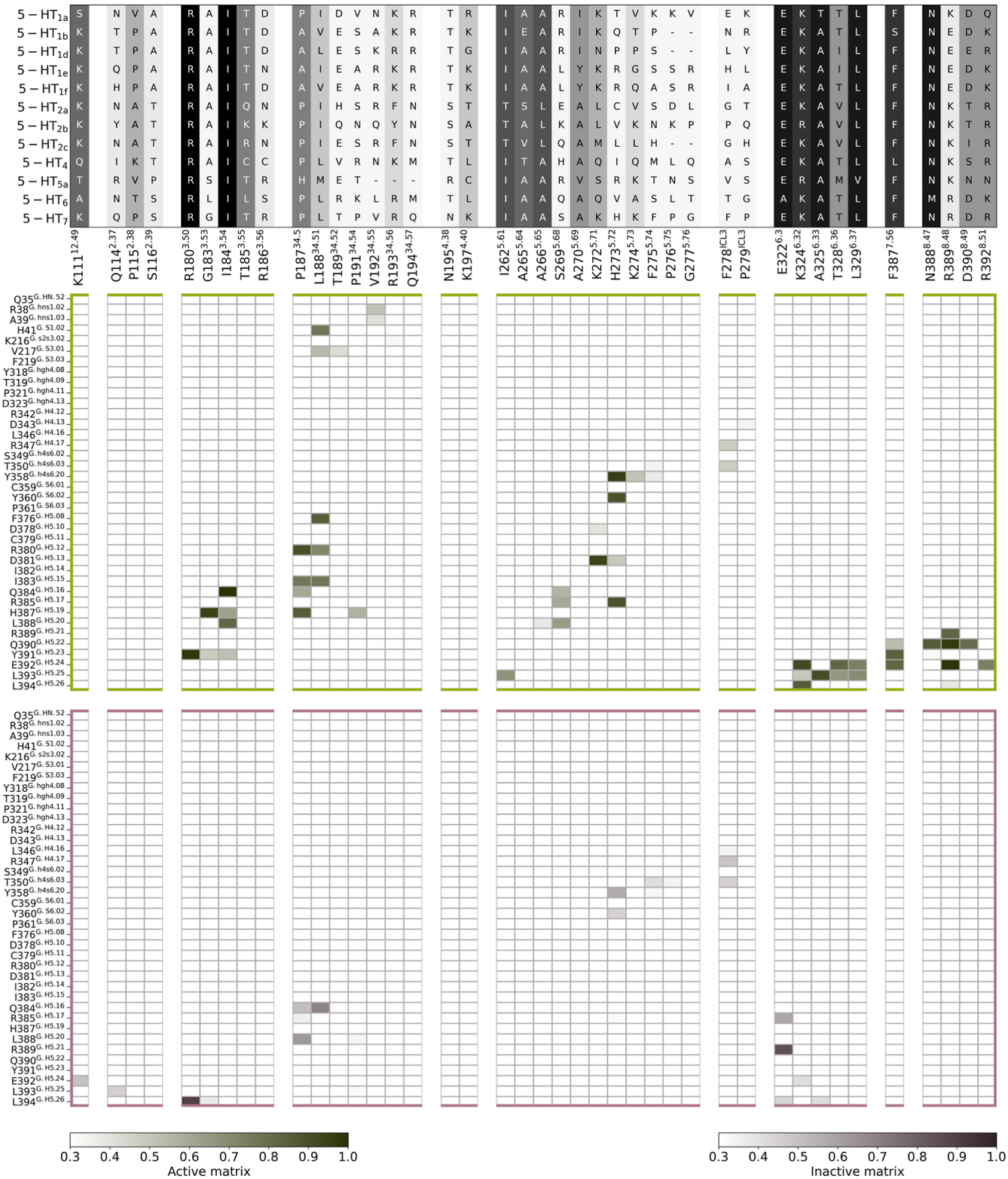

Figure 4. Interaction profiles of active (green framed) and preassembled (purple framed) 5-HT$_7$ in complex with G$_\alpha$ during the MD simulations. 5-HT$_7$ interacting residues are reported in the *x* axis and G protein residues in the *y* axis. Contacts in the structural models are reported in the matrix with green and dark-purple shades for active and preassembled according to the frequency of interactions in the simulations. On the top of the panel, the sequence alignment of 5-HT$_7$ interacting residues to other 5-HT receptors is reported and colored with shades of gray. The matrices of the starting complexes are reported in Figure S8. The per-residue interaction frequencies between 5-HT$_7$ and G$_\alpha$ are mapped onto the structural representation of the proteins in Figure S9.

conserved in class A GPCRs, holding TM3 and TM6 together in the GPCR inactive state. Upon activation, R180$^{3.50}$ swings to interact with the switch Y$^{5.58}$ and Y$^{7.53}$as well as with the G protein.[35] Indeed, the interaction between R180$^{3.50}$ and

https://doi.org/10.1021/acs.jcim.5c01698
J. Chem. Inf. Model. 2025, 65, 11826−11836

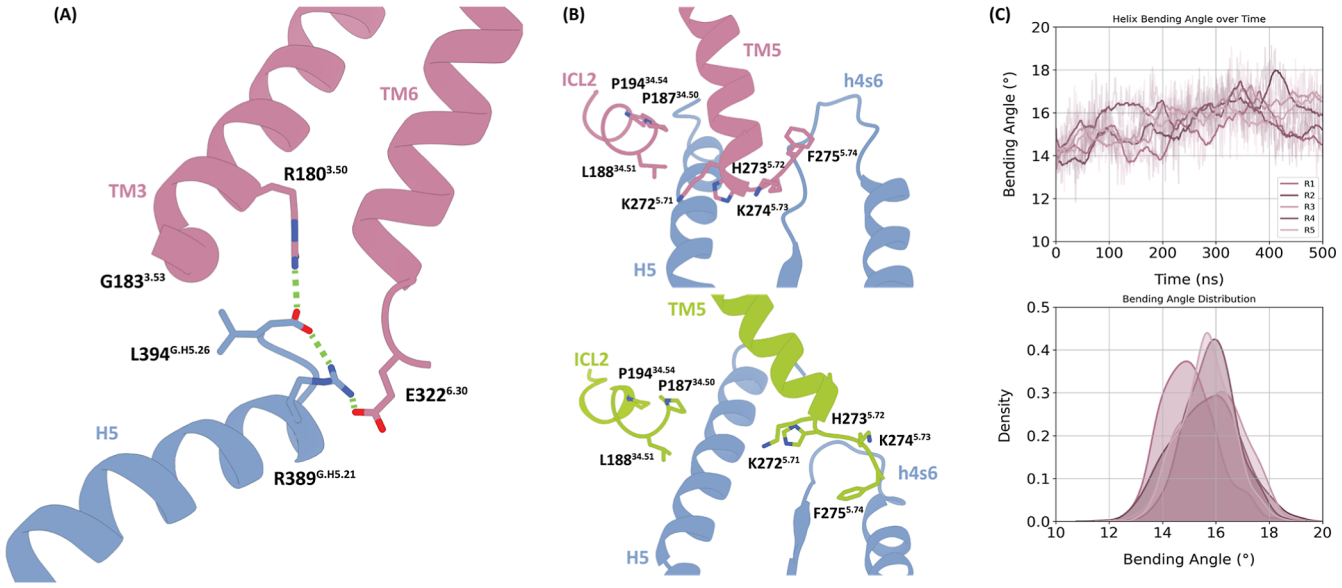

Figure 5. Molecular signature of the preassembled complex. (A) Interaction network between the conserved positions R180$^{3.50}$ and E322$^{6.30}$ of 5-HT$_7$ with R389$^{G.H5.21}$ and L394$^{G.H5.26}$ in H5. Interacting residues are represented as stick and polar interactions with dashed green lines. (B) Structural representation of the interaction between the specific residues driving selectivity TM5 and ICL2 and the G$_s$ in the preassembled (top) and active (bottom) complexes. (C) Time evolution and distribution of the bending angle of the TM5 in the preassembled complex.

Y391$^{G.H5.23}$ is present in our initial active structure and is maintained during simulations.

To analyze the dynamic behavior of these residues in the inactive state of 5-HT$_7$, we run MD simulations (three replicas of 500 ns) for the inactive state model of 5-HT$_7$ without the G$_s$ partner. The RMSD profile of the apo receptor demonstrates overall stability over the course of the simulation (Figure S10). The ionic lock between R180$^{3.50}$ and E322$^{6.30}$, manually introduced in the initial model, is maintained during the simulations of apo inactive 5-HT$_7$ (Figure S10). Instead, it dissociates within the initial 200 ns of all the preassembly replicas (Figure S11) to allow the cytoplasmic region to slightly open up and help G.H5 to form a novel set of interactions: the interactions between E322$^{6.30}$ with R385$^{G.H5.17}$ and R389$^{G.H5.21}$. These interactions are not observed in the active complex nor in the initial preassembly complex but arise only during MD simulations of the preassembled complex.

Here, we propose a mechanism in which the change in interactions of TM3 from the inactive to active state passes through an intermediate conformation stabilized by the preassembled complex with G$_s$. In this intermediate conformation, R180$^{3.50}$ assumes a new conformation and engages in an ionic interaction with the negatively charged C-terminus of L394$^{G.H5.26}$ (Figure 5A). Importantly, L394$^{G.H5.26}$ is in close proximity to G183$^{3.53}$, which is a 5-HT$_7$ specific residue (at this position, other 5-HT receptors have an alanine, leucine, or threonine; see sequence alignment in Figure 4). A larger residue at this position could compromise the interaction between R180$^{3.50}$ and L394$^{G.H5.26}$. Consistent with this, the 3.53 position corresponds to the single nucleotide polymorphism G183$^{3.53}$R, which is predicted to be deleterious (https://gpcrdb.org/protein/5ht7r_human/), underscoring the importance of this position.

The C-terminus of L394$^{G.H5.26}$ establishes an intramolecular ionic lock with R385$^{G.H5.21}$, so that these two residues link TM3 (R180$^{3.50}$) and TM6 (E322$^{6.30}$) together (Figure 5A). The significant role of the interaction between R389$^{G.H5.21}$ and E322$^{6.30}$ in the preassembled complex is in agreement with mutagenesis studies (Ballesteros, Jensen et al. 2001, Liu, Xu et al. 2019). Moreover, in the proposed binding mechanism of the β2-adrenergic receptor to the G$_s$,[36] R389$^{G.H5.21}$ was found to engage in an ionic interaction with D130$^{3.49}$, further supporting the relevance of this residue for the conformational rearrangement leading to the GPCR:G protein active complex.

In addition to interaction patterns involving positions that are conserved in all serotoninergic GPCRs (such as R180$^{3.50}$ and E322$^{6.30}$), our analysis also pinpoints key interactions involving 5-HT$_7$-specific residues (Figure 4). Selective residues in ICL2 (e.g., P191$^{34.54}$) and TM5 (e.g., F275$^{5.74}$) are involved in interaction patterns specific to the active and preassembled states and, therefore, in our proposed activation mechanism (Figure 5B). Importantly, the lengths of TM5 and TM6 were found to vary among the resolved 5-HT receptors, suggesting the relevance of these regions to G protein selectivity.[29]

Residue K274$^{5.73}$ has a stable interaction with Y358$^{G.h4s6.20}$, a contact that is highly specific to the active complex. The entire terminal portion of TM5 (positions 5.71−5.74) forms an extensive interaction network with H5 and h4s6 of the G$_s$ protein, serving to structurally link these domains (Figure 5B, bottom). These interactions are not present in the preassembled starting structure (Figure S8). However, during the simulations, TM5 shifts outward by approximately 16° (Figure 5D). This movement allows it to maintain anchoring interactions with h4s6, but not with H5, indicating a dynamic rearrangement that selectively stabilizes the preassembled complex (Figure 5B, top, Figure 4).

In the preassembled complex, ICL2 residues P187$^{34.50}$, L188$^{34.51}$, and P191$^{34.54}$ are actively involved in interactions with H5 (P187$^{34.50}$ with R385$^{G.H5.17}$ and L388$^{G.H5.20}$, L188$^{34.51}$ with Q384$^{G.H5.16}$, and P191$^{34.54}$ with L388$^{G.H5.20}$ and L393$^{G.H5.25}$), showing over 50% interaction frequencies (Figure 4). However, the interaction network between ICL2 and H5 is broader in the active complex. Additional interactions are observed with residues at the first portion of H5 (F376$^{G.H5.08}$, R380$^{G.H5.12}$, and I383$^{G.H5.15}$), as well as with residues from HN and S3, alongside Q384$^{G.H5.16}$, H387$^{G.H5.19}$, L388$^{G.H5.20}$, and

https://doi.org/10.1021/acs.jcim.5c01698
J. Chem. Inf. Model. 2025, 65, 11826−11836

Y391$^{G.H5.23}$. Previous studies on active GPCR:G_s complexes have shown that the movement of H5 toward ICL2 forms a hydrophobic cavity between the receptor and G protein.[37,38] This cavity can accommodate bulky ICL2 residues and has been suggested to contribute to G_s-coupling specificity.[29] In the 5-HT_7 receptor, this cavity specifically accommodates L188$^{34.51}$. Notably, the presence of a conserved proline (P191$^{34.54}$) in ICL2 can significantly impact the loop dynamics and the orientation of L188$^{34.51}$, likely contributing to the stabilization of this interaction interface.

It should be noted that due to the uncertainty of ICL3 modeling, we excluded this loop from our analyses, despite the fact that it could play a key role in the activation mechanism.[29] The uncertainty of ICL3 modeling[31,32,36,39−41] and the possible variability in TM5 and TM6 length are indeed major challenges of this work, presenting a key area for future investigation. This will be addressed further as new experimental structures covering this area become available.

3. CONCLUSIONS

Using molecular dynamics simulations, we identified stable interaction patterns of the 5-HT_7 receptor in complex with the G protein and highlighted unique structural features distinguishing active, inactive, and preassembled states of the receptor. Notably, the preassembled state reveals a distinct rearrangement of conserved residues R180$^{3.50}$ and E322$^{6.30}$, diverging from the orientation observed in the active and inactive states. This rearrangement supports a mechanistic hypothesis wherein the preassembled complex functions as an intermediate conformation that could facilitate the transition from the inactive to active conformation. Additionally, 5-HT_7-specific ICL2 and TM5 residues appear to play a central role in stabilizing this preassembled architecture, offering new insights into receptor-specific modulation of signaling. Together, these findings propose a model of molecular mechanisms of 5-HT_7 coupling with G_s and underscore the importance of receptor-subtype-specific elements in shaping GPCR signaling properties.

4. METHODS

4.1. Modeling of the Inactive G_s:GDP and Active G_s. MODELLER[44] (AutoModel) was used to reconstruct the missing residues in the GDP-bound G_s protein (PDB ID: 6EG8)(positions 73−86). The active-state $G_{\alpha s}$ protein included mutations K274D, G226A, S54N, T284D, E268A, I285T, R280K, and N271K that were reversed to the wild type using the "Build" tool in Schrodinger. Missing residues (63−208, 253−259) were rebuilt with MODELER (AutoModel) using G_α structures in complex with dopamine and glucagon receptors (PDB IDs: 7JOZ and 6X18, respectively) as templates. Ten models were generated for both the G_s:GDP state and the nucleotide-free state, and the best model was selected based on the DOPE score and visual inspection.

4.2. 3D Structural Modeling of the 5-HT_7 Inactive State and the 5-HT_7:G_s Preassembled Complex. The sequence alignment between 5-HT_7 (UniProtKB: P34969) and serotonin receptors was retrieved from GPCRdb Web server.[42,43] The inactive state of 5-HT_7 was generated based on the active-state experimental structure (PDB ID: 7XTC, resolution of 3.2 Å). The structures of 5-HT_{2A} (PDB ID: 7WC4, resolution of 3.2 Å) and 5-HT_{1B} (PDB ID: 4IAQ, resolution of 2.8 Å) were used as templates to model the regions involved in conformational changes: G77$^{1.28}$−L123$^{2.46}$, A325$^{6.33}$−V338$^{6.46}$, and N380$^{7.49}$−Q402$^{8.61}$. Twenty models were built with MODELER (AutoModel)[44] (v10.2) and the best model was selected based on the DOPE score. For the regions of the 5-HT_7 model where the template information was not available, i.e., residues F275$^{5.74}$−K324$^{6.32}$ and C354−C358 in the ECL3, ab initio modeling was performed using the *loopmodel class* implemented in MODELER.[45] The cysteine residues forming the conserved TM3−ECL2 disulfide bridge[46] (C155$^{3.25}$−C231$^{45.50}$), as well as C354 and C358 in the ECL3, were constrained to form a disulfide bond, as this is shown in the experimental structures of 5-HT_{1a} (PDB ID: 8W8B), 5-HT_{1D} (PDB ID: 7E32), 5-HT_{2b} (PDB ID: 5TUD), 5-HT_{2c} (PDB ID: 6BQH), and 5-HT_6 (PDB ID: 8JLZ) receptors.

We performed loop refinement using both fast and slow algorithms. We built 1000 models for each of the protocols. All the models were aligned with the reference structure (PDB ID: 7E32) retrieved from the OPM database[47] for the correct orientation with the membrane bilayer. We then selected the conformation with minimal clashes with the G_s protein and the membrane. We combined the modeled regions to the experimental structure using the protein splicer tool implemented in Maestro.[48] The final model was minimized to a derivate convergence of 0.01 kJ/mol Å, the OPLS4 force field, and VSGB water solvation model, 65 steps per iteration, using the minimize tool in Bioluminate.[49−51] We then manually changed the rotameric state of R180$^{3.50}$ (similar to that of 6WH4.pdb) to ensure the formation of the ionic lock with E322$^{6.30}$.

Figure S2 provides a representation of the regions modeled with the different approaches.

The preassembled complex was modeled following the approach of Mafi et al.[31] We separately superimposed the inactive state model of 5-HT_7 and inactive G_α, $G_{\beta 1}$, and $G_{\gamma 2}$ to corresponding protein chains in the active state 5-HT_7:G_s complex using the protein structure alignment tool available in Maestro.[48]

4.3. System Preparation of Preassembled and Active Complexes. The preassembled and the active state complexes were prepared using the protein preparation wizard[52] implemented in Maestro.[48] During this protein preparation, the bond orders were assigned, hydrogens were added, and disulfide bonds were created with Epik at pH 7.4 ± 2.0.[53] The hydrogen-bond network of the complexes was optimized with PROPKA,[54] proper protonation state for the optimization of His, Glu, and Asp was monitored using the Interactive optimizer. The residue D127$^{2.50}$ was maintained neutral in the active-state complex and deprotonated for the preassembled complex.[25] Minimization of the hydrogens was performed using the OPLS4 Force Field.[55]

GetContacts (https://getcontacts.github.io/) was used for analysis of the interaction interface between 5-HT_7 and the G_α protein in the active-state complex and the preassembled complex in the initial static structures. By using the get_static_contacts.py tool, we created a list of all the interacting residues at the interface (within 4.5 Å distance). The interface of the preassembled complex involves ICL1 (109$^{1.60}$−116$^{2.39}$), TM3 (152$^{3.22}$−185$^{3.55}$), ICL2 (186$^{3.56}$−195$^{4.38}$), TM5 (237$^{5.36}$−272$^{5.71}$), ICL3 (273$^{5.72}$−320$^{6.28}$), TM6 (321$^{6.29}$−349$^{6.57}$), and H8 (389$^{8.48}$−402$^{8.61}$) of 5-HT_7, and αN, α5, α4, β1, β2, β6, and H4S6 regions of the G_α protein. Next, using the "*get_contact_frequencies.py*" module, we calculated the frequency of each interaction found in the

https://doi.org/10.1021/acs.jcim.5c01698
J. Chem. Inf. Model. 2025, 65, 11826−11836

contact list such as polar interactions (hydrogen bonds, salt bridges) and nonpolar interactions (Hydrophobic, π-stacking, T-stacking, and π-cation).

Homolwat Web server[56] was used to add water molecules within the receptor structures, applying settings described in the GPCRmd protocol.[25] The orientation of the prepared complexes within the membrane bilayer was obtained from the coordinates of the 5-HT_{1D} receptor (PDB ID: 7E32), as deposited in the Orientations of Proteins in Membranes (OPM) database.[57] The two complexes were superimposed on the X-ray irradiation of the OPM reference structure. The prepared complexes were then embedded into a prebuilt (with VMD Membrane Builder plugin 1.1) 1-palmitoyl-2oleyl-*sn*-glycerol-3-phospho-choline (POPC) square bilayer of 131 Å × 131 Å × 165 Å and 143 Å × 143 Å × 160 Å for active and preassembled complexes, respectively, through an insertion method[58] by using HTMD[59] (Acellera, version 2.0.8). Lipids overlapping with protein residues were removed. TIP3P water molecules were added to the simulation boxes by using VMD Solvate plugin 1.5. The overall charge neutrality was maintained by adding Na^+/Cl^- ions to reach a final physiological concentration of 0.154 M by using VMD Autonize plugin 1.3. All the N- and C-terminus chains (GPCR, G_α, G_β, G_γ) were capped with ACE and CT3, with the exception of G_α helix 5 ($L394^{H5.26}$), which remained negatively charged. This preparation protocol was also applied for the system preparation of the 5-HT_7 inactive state (with full ICL3) without the heterotrimeric G protein. The difference relies on the membrane size. Here, we embedded the inactive GPCR into a 1-palmitoyl-2oleyl-*sn*-glycerol-3-phospho-choline (POPC) square bilayer of 120 Å × 120 Å. TIP3P water molecules were added to the 116 Å × 116 Å × 126 Å simulation box with the same concentration of counterions.

4.4. MD Simulation Protocol and Analyses. The CgenFF[60] (v4.6) and CHARMM36[61,62] for protein, lipid, TIP3P water model, GDP, and nucleic acid were used for this work. The topology and parameters of the cocrystallized ligand (5-Carboxamidotryptamine, 5-CT) in 7XTC were obtained from the ParamChem Web server (https://cgenff.umaryland.edu/). We simulated three systems: 5-CT:5-HT_7:G_s, preassembled complex 5-HT_7:G_s:GDP, and 5-HT_7 inactive state without the G-protein (Table S1).

ACEMD[63] (Acellera, version 3.5.1) was used for MD simulations with periodic boundary conditions. The systems were initially equilibrated through a 5000 conjugate gradient step minimization to reduce clashes induced by the system preparation between protein and lipid/water atoms and then equilibrated with 120 ns MD simulation in the isothermal−isobaric conditions (*NPT* ensemble), employing an integration step of 2 fs. The temperature was maintained at 310 K using a Langevin thermostat[64] with a low damping constant of 1 ps^{-1}, and the pressure was maintained at 1.01325 atm using a Monte Carlo barostat. Initial restraints of 5 kcal mol^{-1} $Å^{-2}$ were gradually reduced in a multistage procedure over the 120 ns: 6 ns for lipid phosphorus atoms, 90 ns for all protein atoms other than C_α atoms, 100 ns for the protein C_α atoms, and 120 ns for GDP or cocrystallized ligand. The M-SHAKE algorithm[65] was used to constrain the bond lengths involving hydrogen atoms. Long-range Columbic interactions were handled using the particle mesh Ewald summation method[66] with a grid size rounded to the approximate integer value of cell wall dimensions. The cutoff distance for long-term interactions was set at 9.0 Å, with a switching function of 7.5 Å.

To evaluate the stability and the biophysical validity of the equilibrated systems, the average area per lipid (ApL) headgroup with VTMC,[67] the bilayer thickness with MEMPLUGIN,[68] and the volume of the simulation box were calculated. The computed ApL and thickness were in agreement with the experimental values measured for the POPC lipid bilayers. We run five independent replicas for each equilibrated system of 500 ns unrestrained MD simulations in the canonical ensemble (*NVT*) with an integration time step of 4 fs. The temperature was set at 310 K, by setting the damping constant at 0.1 ps^{-1}.

RMSD and RMSF of the backbone carbon alpha were computed for each chain (GPCR, G_α, G_β, G_γ) with an in-house python script based on MDAnalysis (v2.2.0).[69] We used as a reference the starting structures. We computed the RMSD using two types of alignment: first, chain-to-chain alignment (the ICL3 region of 5-HT_7 and G_α residue 64−87 were excluded from the alignment); second, we used as a reference the GPCR carbon alpha atoms excluding the ICL3 region. To compute the RMSF, we used chain-to-chain alignment. The 5-HT_7 active structure was used as a reference for both aligning and computing the RMSD values of $R385^{G.H5.17}$ and $Y391^{G.H5.21}$.

For the analysis of the interactions of the MD simulations, the five replicas for each system were merged into a single trajectory. Given the uncertainty in modeling the ICL3 region, we selected a conformation that did not interfere with the G protein. These rebuilt residues were excluded from subsequent analyses. MDciao python module (v0.5)[70] (https://github.com/gph82/mdciao) was used to calculate and compute the interaction frequencies between the GPCR and the G_α. We set the cutoff to 4 Å and computed a number of maximum contacts of 80, excluding the first 100 ns of each replica. The distance of the salt bridge between residues $R180^{3.50}$ and $E322^{6.30}$ was monitored using the distance between the CG atom of $E322^{3.50}$ and the CZ atom of $R180^{3.50}$, calculated with the module "*distances.distance_array*" in MDAnalysis (v2.2.0).[69]

To evaluate conformational changes in TM5 across different replicas of the preassembled complex, we computed the bending angle (θ) from the positions of C_α in two consecutive residue segments along TM5. We define two vectors: (i) Vector 1 ($\vec{v}_1$): from the first to the last C_α atom of residues $F237^{5.36}$−$Y249^{5.48}$ (extracellular portion), (ii) Vector 2 ($\vec{v}_2$): from the first to the last C_α atom of residues $I250^{5.49}$−$H273^{5.72}$ (intracellular portion). The bending angle θ at each simulation frame was computed by using the dot product of the normalized vectors:

$$\theta = \frac{\vec{v}_1 \cdot \vec{v}_2}{\|\vec{v}_1\| \|\vec{v}_2\|} \quad (1)$$

where the $\vec{v}_1 \cdot \vec{v}_2$ denotes the dot product and $\|\vec{v}_i\|$ is the Euclidean norm of $\vec{v}_i$. The calculation was computed across every frame of each trajectory using MDAnalysis (v2.2.0).[69] Rendering of the structural images was done with ChimeraX (v1.9).[71] Visualization of all data was done with the Matplotlib and seaborn Python library.[72,73]

■ ASSOCIATED CONTENT

Data Availability Statement

Topology, parameter, and coordinate files as well as MD trajectories are available at https://zenodo.org/records/

https://doi.org/10.1021/acs.jcim.5c01698
J. Chem. Inf. Model. 2025, 65, 11826−11836

15195899. The MD simulation of system 1 have been deposited into the GPCRmd database (https://www.gpcrmd.org/) under access codes 2370 (https://www.gpcrmd.org/view/2370/).

Supporting Information

The Supporting Information is available free of charge at https://pubs.acs.org/doi/10.1021/acs.jcim.5c01698.

Heterotrimeric G_s protein representations, representation of the 5-HT_7 refined models, electrostatic surface of 5HT_7:G_s complexes, RMSD and RMSF analyses, H5 conformational space, and distance plot of ionic lock (PDF)

AUTHOR INFORMATION

Corresponding Authors

Alessandro Nicoli − *Leibniz Institute for Food Systems Biology at the Technical University of Munich, Freising 85354, Germany; Professorship for Chemoinformatics and Protein Modelling, TUM School of Life Sciences, Technical University of Munich, 85354 Freising, Germany;* orcid.org/0000-0001-6177-9749; Phone: +498161716517; Email: a.nicoli.leibniz-lsb@tum.de

Antonella Di Pizio − *Leibniz Institute for Food Systems Biology at the Technical University of Munich, Freising 85354, Germany; Professorship for Chemoinformatics and Protein Modelling, TUM School of Life Sciences, Technical University of Munich, 85354 Freising, Germany;* orcid.org/0000-0002-8520-5165; Phone: +498161716516; Email: a.dipizio.leibniz-lsb@tum.de

Authors

Zeenat Zara − *Leibniz Institute for Food Systems Biology at the Technical University of Munich, Freising 85354, Germany; Faculty of Science, University of South Bohemia in Ceske Budejovice, Ceske Budejovice 370 05, Czech Republic*

Ruiming He − *Leibniz Institute for Food Systems Biology at the Technical University of Munich, Freising 85354, Germany; Center for Functional Protein Assemblies (CPA), Department Bioscience, TUM School of Natural Science, Technical University of Munich, Garching 85748, Germany*

Natalia Kulik − *Laboratory of Photosynthesis, Centre Algatech, Institute of Microbiology of the Czech Academy of Sciences, Třeboň CZ-37981, Czech Republic;* orcid.org/0000-0003-2005-8165

David Reha − *IT4Innovations, VSB—Technical University of Ostrava, Ostrava-Poruba 708 00, Czech Republic*

Alexey Bondar − *Faculty of Science, University of South Bohemia in Ceske Budejovice, Ceske Budejovice 370 05, Czech Republic; Institute of Plant Molecular Biology, Biology Centre of the Czech Academy of Sciences, Ceske Budejovice 370 05, Czech Republic;* orcid.org/0000-0002-1980-2930

Complete contact information is available at: https://pubs.acs.org/10.1021/acs.jcim.5c01698

Author Contributions

[▽]Z.Z. and A.N. contributed equally to this work. All authors contributed to the manuscript. Conceptualization: A.N., A.B., A.D.P. Project supervision: A.N., A.D.P. Methodology: Z.Z., A.N., A.D.P. Formal analysis: Z.Z., A.N., R.H. Writing—original draft: Z.Z., A.N., R.H., N.K., A.B., D.R., A.D.P. Writing—Review and editing: Z.Z., A.N., R.H., N.K., A.B., D.R., A.D.P. Resources and Project administrations: A.D.P. Visualization: Z.Z. A.N. All authors read and approved the final manuscript.

Notes

The authors declare no competing financial interest.

ACKNOWLEDGMENTS

A.N., A.B., and A.D.P. are members of the GPCRforum (https://www.gpcrforum.org/home). The research of A.D.P. is supported by the Leibniz Programme for Women Professors (grant: P116/2020) and the Alzheimer's Association (grant: AARG-23-1141447).

REFERENCES

(1) Guseva, D.; Wirth, A.; Ponimaskin, E. Cellular mechanisms of the 5-HT7 receptor-mediated signaling. *Front. Behav. Neurosci.* **2014**, *8*, 306.

(2) Hedlund, P. B.; Sutcliffe, J. G. Functional, molecular and pharmacological advances in 5-HT7 receptor research. *Trends Pharmacol. Sci.* **2004**, *25*, 481−486.

(3) Blattner, K. M.; Canney, D. J.; Pippin, D. A.; Blass, B. E. Pharmacology and therapeutic potential of the 5-HT7 receptor. *ACS Chem. Neurosci.* **2019**, *10*, 89−119.

(4) Dogrul, A.; Seyrek, M. Systemic morphine produce antinociception mediated by spinal 5-HT7, but not 5-HT1A and 5-HT2 receptors in the spinal cord. *Br. J. Pharmacol.* **2006**, *149*, 498−505.

(5) Matthys, A.; Haegeman, G.; Van Craenenbroeck, K.; Vanhoenacker, P. Role of the 5-HT7 receptor in the central nervous system: from current status to future perspectives. *Mol. Neurobiol.* **2011**, *43*, 228−253.

(6) Quintero-Villegas, A.; Valdés-Ferrer, S. I. Role of 5-HT7 receptors in the immune system in health and disease. *Mol. Med.* **2020**, *26*, 2.

(7) Quintero-Villegas, A.; Valdés-Ferrer, S. I. Central nervous system effects of 5-HT7 receptors: a potential target for neurodegenerative diseases. *Mol. Med.* **2022**, *28*, 70.

(8) Scharf, M. M.; Humphrys, L. J.; Berndt, S.; Di Pizio, A.; Lehmann, J.; Liebscher, I.; Nicoli, A.; Niv, M. Y.; Peri, L.; Schihada, H.; Schulte, G. The dark sides of the GPCR tree-research progress on understudied GPCRs. *Br. J. Pharmacol.* **2025**, *182*, 3109−3134.

(9) Yang, D.; Zhou, Q.; Labroska, V.; Qin, S.; Darbalaei, S.; Wu, Y.; Yuliantie, E.; Xie, L.; Tao, H.; Cheng, J.; Liu, Q.; Zhao, S.; Shui, W.; Jiang, Y.; Wang, M. W. G protein-coupled receptors: structure- and function-based drug discovery. *Signal Transduction Targeted Ther.* **2021**, *6*, 7.

(10) Sharp, T.; Barnes, N. M. Central 5-HT receptors and their function; present and future. *Neuropharmacology* **2020**, *177*, 108155.

(11) Kogut-Gunthel, M. M.; Zara, Z.; Nicoli, A.; Steuer, A.; Lopez-Balastegui, M.; Selent, J.; Karanth, S.; Koehler, M.; Ciancetta, A.; Abiko, L. A.; Hagn, F.; Di Pizio, A. The path to the G protein-coupled receptor structural landscape: Major milestones and future directions. *Br. J. Pharmacol.* **2025**, *182*, 3225−3248.

(12) Conflitti, P.; Lyman, E.; Sansom, M. S. P.; Hildebrand, P. W.; Gutierrez-de-Teran, H.; Carloni, P.; Ansell, T. B.; Yuan, S.; Barth, P.; Robinson, A. S.; Tate, C. G.; Gloriam, D.; Grzesiek, S.; Eddy, M. T.; Prosser, S.; Limongelli, V. Functional dynamics of G protein-coupled receptors reveal new routes for drug discovery. *Nat. Rev. Drug Discovery* **2025**, *24*, 251−275.

(13) Syrovatkina, V.; Alegre, K. O.; Dey, R.; Huang, X. Y. Regulation, Signaling, and Physiological Functions of G-Proteins. *J. Mol. Biol.* **2016**, *428*, 3850−3868.

(14) Nichols, D. E.; Nichols, C. D. Serotonin receptors. *Chem. Rev.* **2008**, *108*, 1614−1641.

(15) Nobles, M.; Benians, A.; Tinker, A. Heterotrimeric G proteins precouple with G protein-coupled receptors in living cells. *Proc. Natl. Acad. Sci. U.S.A.* **2005**, *102*, 18706−18711.
(16) Galés, C.; Van Durm, J. J.; Schaak, S.; Pontier, S.; Percherancier, Y.; Audet, M.; Paris, H.; Bouvier, M. Probing the activation-promoted structural rearrangements in preassembled receptor−G protein complexes. *Nat. Struct. Mol. Biol.* **2006**, *13*, 778−786.
(17) Qin, K.; Dong, C.; Wu, G.; Lambert, N. A. Inactive-state preassembly of Gq-coupled receptors and Gq heterotrimers. *Nat. Chem. Biol.* **2011**, *7*, 740−747.
(18) Andressen, K. W.; Ulsund, A. H.; Krobert, K. A.; Lohse, M. J.; Buenemann, M.; Levy, F. O. Related GPCRs couple differently to Gs: preassociation between G protein and 5-HT7 serotonin receptor reveals movement of Gαs upon receptor activation. *FASEB J.* **2018**, *32*, 1059−1069.
(19) Jang, W.; Adams, C. E.; Liu, H.; Zhang, C.; Levy, F. O.; Andressen, K. W.; Lambert, N. A. An inactive receptor-G protein complex maintains the dynamic range of agonist-induced signaling. *Proc. Natl. Acad. Sci. U.S.A.* **2020**, *117*, 30755−30762.
(20) Damian, M.; Mary, S.; Maingot, M.; M'Kadmi, C.; Gagne, D.; Leyris, J. P.; Denoyelle, S.; Gaibelet, G.; Gavara, L.; Garcia de Souza Costa, M.; Perahia, D.; Trinquet, E.; Mouillac, B.; Galandrin, S.; Gales, C.; Fehrentz, J. A.; Floquet, N.; Martinez, J.; Marie, J.; Baneres, J. L. Ghrelin receptor conformational dynamics regulate the transition from a preassembled to an active receptor:Gq complex. *Proc. Natl. Acad. Sci. U.S.A.* **2015**, *112*, 1601−1606.
(21) Ayoub, M. A.; Trinquet, E.; Pfleger, K. D.; Pin, J. P. Differential association modes of the thrombin receptor PAR1 with Galphai1, Galpha12, and beta-arrestin 1. *FASEB J.* **2010**, *24*, 3522−3535.
(22) Petelak, A.; Lambert, N. A.; Bondar, A. Serotonin 5-HT(7) receptor slows down the G(s) protein: a single molecule perspective. *Mol. Biol. Cell* **2023**, *34*, br14.
(23) Civciristov, S.; Ellisdon, A. M.; Suderman, R.; Pon, C. K.; Evans, B. A.; Kleifeld, O.; Charlton, S. J.; Hlavacek, W. S.; Canals, M.; Halls, M. L. Preassembled GPCR signaling complexes mediate distinct cellular responses to ultralow ligand concentrations. *Sci. Signaling* **2018**, *11*, No. eaan1188.
(24) Shao, Z.; Dong, Y.; Jia, R.; Shen, Q.; Yao, B.; He, X.; Yuan, Q.; Shen, D.; Mao, C.; Zhang, C.; Chen, Z.; Eric Xu, H.; Ying, S.; Zhang, Y.; Li, W. Structural basis of GPCR-G protein pre-coupling and activation: insights from CCR1-Gi complex. *bioRxiv* **2024**, 2024.11.01.621549.
(25) Aranda-Garcia, D.; Stepniewski, T. M.; Torrens-Fontanals, M.; Garcia-Recio, A.; Lopez-Balastegui, M.; Medel-Lacruz, B.; Morales-Pastor, A.; Peralta-Garcia, A.; Dieguez-Eceolaza, M.; Sotillo-Nunez, D.; Ding, T.; Drabek, M.; Jacquemard, C.; Jakowiecki, J.; Jespers, W.; Jimenez-Roses, M.; Jun-Yu-Lim, V.; Nicoli, A.; Orzel, U.; Shahraki, A.; Tiemann, J. K. S.; Ledesma-Martin, V.; Nerin-Fonz, F.; Suarez-Dou, S.; Canal, O.; Pandy-Szekeres, G.; Mao, J.; Gloriam, D. E.; Kellenberger, E.; Latek, D.; Guixa-Gonzalez, R.; Gutierrez-de-Teran, H.; Tikhonova, I. G.; Hildebrand, P. W.; Filizola, M.; Babu, M. M.; Di Pizio, A.; Filipek, S.; Kolb, P.; Cordomi, A.; Giorgino, T.; Marti-Solano, M.; Selent, J. Large scale investigation of GPCR molecular dynamics data uncovers allosteric sites and lateral gateways. *Nat. Commun.* **2025**, *16*, 2020.
(26) Lopez-Balastegui, M.; Stepniewski, T. M.; Kogut-Gunthel, M. M.; Di Pizio, A.; Rosenkilde, M. M.; Mao, J.; Selent, J. Relevance of G protein-coupled receptor (GPCR) dynamics for receptor activation, signalling bias and allosteric modulation. *Br. J. Pharmacol.* **2025**, *182*, 3211−3224.
(27) Liu, X.; Xu, X.; Hilger, D.; Aschauer, P.; Tiemann, J. K.; Du, Y.; Liu, H.; Hirata, K.; Sun, X.; Guixà-González, R.; et al. Structural insights into the process of GPCR-G protein complex formation. *Cell* **2019**, *177*, 1243−1251.e12.
(28) Ballesteros, J. A.; Weinstein, H. [19] Integrated methods for the construction of three-dimensional models and computational probing of structure-function relations in G protein-coupled receptors. *Methods in Neurosciences*; Elsevier, 1995; Vol. *25*, pp 366−428.
(29) Huang, S.; Xu, P.; Shen, D.-D.; Simon, I. A.; Mao, C.; Tan, Y.; Zhang, H.; Harpsøe, K.; Li, H.; Zhang, Y.; et al. GPCRs steer Gi and Gs selectivity via TM5-TM6 switches as revealed by structures of serotonin receptors. *Mol. Cell* **2022**, *82*, 2681−2695.e6.
(30) Mafi, A.; Kim, S.-K.; Goddard, W. A., III The dynamics of agonist-β2-adrenergic receptor activation induced by binding of GDP-bound Gs protein. *Nat. Chem.* **2023**, *15*, 1127−1137.
(31) Mafi, A.; Kim, S.-K.; Goddard, W. A., III The mechanism for ligand activation of the GPCR−G protein complex. *Proc. Natl. Acad. Sci. U.S.A.* **2022**, *119*, No. e2110085119.
(32) Papasergi-Scott, M. M.; Perez-Hernandez, G.; Batebi, H.; Gao, Y.; Eskici, G.; Seven, A. B.; Panova, O.; Hilger, D.; Casiraghi, M.; He, F.; Maul, L.; Gmeiner, P.; Kobilka, B. K.; Hildebrand, P. W.; Skiniotis, G. Time-resolved cryo-EM of G-protein activation by a GPCR. *Nature* **2024**, *629*, 1182−1191.
(33) Hollingsworth, S. A.; Dror, R. O. Molecular Dynamics Simulation for All. *Neuron* **2018**, *99*, 1129−1143.
(34) Zhou, Q.; Yang, D.; Wu, M.; Guo, Y.; Guo, W.; Zhong, L.; Cai, X.; Dai, A.; Jang, W.; Shakhnovich, E. I.; Liu, Z. J.; Stevens, R. C.; Lambert, N. A.; Babu, M. M.; Wang, M. W.; Zhao, S. Common activation mechanism of class A GPCRs. *Elife* **2019**, *8*, No. e50279.
(35) Carpenter, B.; Tate, C. G. Active state structures of G protein-coupled receptors highlight the similarities and differences in the G protein and arrestin coupling interfaces. *Curr. Opin. Struct. Biol.* **2017**, *45*, 124−132.
(36) Batebi, H.; Perez-Hernandez, G.; Rahman, S. N.; Lan, B.; Kamprad, A.; Shi, M.; Speck, D.; Tiemann, J. K. S.; Guixa-Gonzalez, R.; Reinhardt, F.; Stadler, P. F.; Papasergi-Scott, M. M.; Skiniotis, G.; Scheerer, P.; Kobilka, B. K.; Mathiesen, J. M.; Liu, X.; Hildebrand, P. W. Mechanistic insights into G-protein coupling with an agonist-bound G-protein-coupled receptor. *Nat. Struct. Mol. Biol.* **2024**, *31*, 1692−1701.
(37) Du, Y.; Duc, N. M.; Rasmussen, S. G. F.; Hilger, D.; Kubiak, X.; Wang, L.; Bohon, J.; Kim, H. R.; Wegrecki, M.; Asuru, A.; Jeong, K. M.; Lee, J.; Chance, M. R.; Lodowski, D. T.; Kobilka, B. K.; Chung, K. Y. Assembly of a GPCR-G Protein Complex. *Cell* **2019**, *177*, 1232−1242 e11.
(38) Zhuang, Y.; Xu, P.; Mao, C.; Wang, L.; Krumm, B.; Zhou, X. E.; Huang, S.; Liu, H.; Cheng, X.; Huang, X. P.; Shen, D. D.; Xu, T.; Liu, Y. F.; Wang, Y.; Guo, J.; Jiang, Y.; Jiang, H.; Melcher, K.; Roth, B. L.; Zhang, Y.; Zhang, C.; Xu, H. E. Structural insights into the human D1 and D2 dopamine receptor signaling complexes. *Cell* **2021**, *184*, 931−942 e18.
(39) Sadler, F.; Ma, N.; Ritt, M.; Sharma, Y.; Vaidehi, N.; Sivaramakrishnan, S. Autoregulation of GPCR signalling through the third intracellular loop. *Nature* **2023**, *615*, 734−741.
(40) Deganutti, G.; Pipito, L.; Rujan, R. M.; Weizmann, T.; Griffin, P.; Ciancetta, A.; Moro, S.; Reynolds, C. A. Hidden GPCR structural transitions addressed by multiple walker supervised molecular dynamics (mwSuMD). *Elife* **2025**, *13*, RP96513.
(41) Sandhu, M.; Cho, A.; Ma, N.; Mukhaleva, E.; Namkung, Y.; Lee, S.; Ghosh, S.; Lee, J. H.; Gloriam, D. E.; Laporte, S. A.; Babu, M. M.; Vaidehi, N. Dynamic spatiotemporal determinants modulate GPCR:G protein coupling selectivity and promiscuity. *Nat. Commun.* **2022**, *13*, 7428.
(42) Pándy-Szekeres, G.; Esguerra, M.; Hauser, A. S.; Caroli, J.; Munk, C.; Pilger, S.; Keserű, G. M.; Kooistra, A. J.; Gloriam, D. E. The G protein database, GproteinDb. *Nucleic Acids Res.* **2022**, *50*, D518−D525.
(43) PDB PDB. https://www.rcsb.org/structure/7XTC. 06.08.2022
(44) Šali, A.; Blundell, T. L. Comparative protein modelling by satisfaction of spatial restraints. *J. Mol. Biol.* **1993**, *234*, 779−815.
(45) Fiser, A.; Do, R. K.; Sali, A. Modeling of loops in protein structures. *Protein Sci.* **2000**, *9*, 1753−1773.
(46) Nicoli, A.; Dunkel, A.; Giorgino, T.; de Graaf, C.; Di Pizio, A. Classification Model for the Second Extracellular Loop of Class A GPCRs. *J. Chem. Inf. Model.* **2022**, *62*, 511−522.
(47) Lomize, M. A.; Pogozheva, I. D.; Joo, H.; Mosberg, H. I.; Lomize, A. L. OPM database and PPM web server: resources for

positioning of proteins in membranes. *Nucleic Acids Res.* **2012**, *40*, D370−D376.
(48) Maestro, S. *Maestro*; Schrödinger LLC: New York, NY, 2020.
(49) Zhu, K.; Day, T.; Warshaviak, D.; Murrett, C.; Friesner, R.; Pearlman, D. Antibody structure determination using a combination of homology modeling, energy-based refinement, and loop prediction. *Proteins: Struct., Funct., Bioinf.* **2014**, *82*, 1646−1655.
(50) Negron, C.; Fang, J.; McPherson, M. J.; Stine, W. B., Jr; McCluskey, A. J. Separating clinical antibodies from repertoire antibodies, a path to in silico developability assessment. *mAbs* **2022**, *14*, 2080628.
(51) Beard, H.; Cholleti, A.; Pearlman, D.; Sherman, W.; Loving, K. A. Applying physics-based scoring to calculate free energies of binding for single amino acid mutations in protein-protein complexes. *PLoS One* **2013**, *8*, No. e82849.
(52) Madhavi Sastry, G.; Adzhigirey, M.; Day, T.; Annabhimoju, R.; Sherman, W. Protein and ligand preparation: parameters, protocols, and influence on virtual screening enrichments. *J. Comput.-Aided Mol. Des.* **2013**, *27*, 221−234.
(53) Greenwood, J. R.; Calkins, D.; Sullivan, A. P.; Shelley, J. C. Towards the comprehensive, rapid, and accurate prediction of the favorable tautomeric states of drug-like molecules in aqueous solution. *J. Comput.-Aided Mol. Des.* **2010**, *24*, 591−604.
(54) Olsson, M. H.; Søndergaard, C. R.; Rostkowski, M.; Jensen, J. H. PROPKA3: consistent treatment of internal and surface residues in empirical p K a predictions. *J. Chem. Theory Comput.* **2011**, *7*, 525−537.
(55) Lu, C.; Wu, C.; Ghoreishi, D.; Chen, W.; Wang, L.; Damm, W.; Ross, G. A.; Dahlgren, M. K.; Russell, E.; Von Bargen, C. D.; et al. OPLS4: Improving force field accuracy on challenging regimes of chemical space. *J. Chem. Theory Comput.* **2021**, *17*, 4291−4300.
(56) Mayol, E.; García-Recio, A.; Tiemann, J. K.; Hildebrand, P. W.; Guixà-González, R.; Olivella, M.; Cordomí, A. HomolWat: a web server tool to incorporate 'homologous' water molecules into GPCR structures. *Nucleic Acids Res.* **2020**, *48*, W54−W59.
(57) Lomize, M. A.; Lomize, A. L.; Pogozheva, I. D.; Mosberg, H. I. OPM: orientations of proteins in membranes database. *Bioinformatics* **2006**, *22*, 623−625.
(58) Sommer, B. Membrane packing problems: a short review on computational membrane modeling methods and tools. *Comput. Struct. Biotechnol. J.* **2013**, *5*, No. e201302014.
(59) Doerr, S.; Harvey, M.; Noé, F.; De Fabritiis, G. HTMD: high-throughput molecular dynamics for molecular discovery. *J. Chem. Theory Comput.* **2016**, *12*, 1845−1852.
(60) Stipp, S.; Eggleston, C.; Nielsen, B. Calcite surface structure observed at microtopographic and molecular scales with atomic force microscopy (AFM). *Geochim. Cosmochim. Acta* **1994**, *58*, 3023−3033.
(61) Huang, J.; Rauscher, S.; Nawrocki, G.; Ran, T.; Feig, M.; De Groot, B. L.; Grubmüller, H.; MacKerell Jr, A. D. CHARMM36m: an improved force field for folded and intrinsically disordered proteins. *Nat. Methods* **2017**, *14*, 71−73.
(62) Huang, J.; MacKerell Jr, A. D. CHARMM36 all-atom additive protein force field: Validation based on comparison to NMR data. *J. Comput. Chem.* **2013**, *34*, 2135−2145.
(63) Harvey, M. J.; Giupponi, G.; Fabritiis, G. D. ACEMD: accelerating biomolecular dynamics in the microsecond time scale. *J. Chem. Theory Comput.* **2009**, *5*, 1632−1639.
(64) Loncharich, R. J.; Brooks, B. R.; Pastor, R. W. Langevin dynamics of peptides: The frictional dependence of isomerization rates of N-acetylalanyl-N′-methylamide. *Biopolymers* **1992**, *32*, 523−535.
(65) Kräutler, V.; Van Gunsteren, W. F.; Hünenberger, P. H. A fast SHAKE algorithm to solve distance constraint equations for small molecules in molecular dynamics simulations. *J. Comput. Chem.* **2001**, *22*, 501−508.
(66) Essmann, U.; Perera, L.; Berkowitz, M. L.; Darden, T.; Lee, H.; Pedersen, L. G. A smooth particle mesh Ewald method. *J. Chem. Phys.* **1995**, *103*, 8577−8593.
(67) Gapsys, V.; de Groot, B. L.; Briones, R. Computational analysis of local membrane properties. *J. Comput.-Aided Mol. Des.* **2013**, *27*, 845−858.
(68) Guixà-González, R.; Rodriguez-Espigares, I.; Ramírez-Anguita, J. M.; Carrió-Gaspar, P.; Martinez-Seara, H.; Giorgino, T.; Selent, J. MEMBPLUGIN: studying membrane complexity in VMD. *Bioinformatics* **2014**, *30*, 1478−1480.
(69) Michaud-Agrawal, N.; Denning, E. J.; Woolf, T. B.; Beckstein, O. MDAnalysis: a toolkit for the analysis of molecular dynamics simulations. *J. Comput. Chem.* **2011**, *32*, 2319−2327.
(70) Perez-Hernandez, G.; Hildebrand, P. W. mdciao: Accessible Analysis and Visualization of Molecular Dynamics Simulation Data. *PLoS Comput. Biol.* **2025**, *21*, No. e1012837.
(71) Meng, E. C.; Goddard, T. D.; Pettersen, E. F.; Couch, G. S.; Pearson, Z. J.; Morris, J. H.; Ferrin, T. E. UCSF ChimeraX: Tools for structure building and analysis. *Protein Sci.* **2023**, *32*, No. e4792.
(72) Hunter, J. D. Matplotlib: A 2D Graphics Environment. *Comput. Sci. Eng.* **2007**, *9*, 90−95.
(73) Waskom, M. Seaborn: statistical data visualization. *J. Open Source Softw.* **2021**, *6*, 3021.

https://doi.org/10.1021/acs.jcim.5c01698
J. Chem. Inf. Model. 2025, 65, 11826−11836